SCIENTIFIC REPORTS

OPEN

Opposite-view digital holographic microscopy with autofocusing capability

Received: 26 January 2017
Accepted: 16 May 2017
Published online: 26 June 2017

Juanjuan Zheng[1], Peng Gao[2,3] & Xiaopeng Shao[1]

Digital holographic microscopy (DHM) has its intrinsic ability to refocusing a sample by numerically propagating an object wave from its hologram plane to its image plane. In this paper opposite-view digital holographic microscopy (OV-DHM) is demonstrated for autofocusing, namely, digitally determining the location of the image plane, and refocusing the object wave without human intervention. In OV-DHM, a specimen is illuminated from two sides in a 4π-alike configuration, and two holograms are generated and recorded by a CCD camera along two orthogonal polarization orientations. The image plane of the sample is determined by finding the minimal variation between the two object waves, and consequently refocusing is performed by propagating the waves to the image plane. Furthermore, the field of view (FOV) of OV-DHM can be extended by combining the two object waves which have an angle in-between. The proposed technique also has the potential to reduce speckle noise and out-of-focus background.

Digital holographic microscopy (DHM) is a non-invasive, high-resolution, whole-field technique for measuring microscopic specimens, especially translucent sample.[1–5] In microcopy, samples are often observed in in-focus scene through manual or mechanical focusing. However, this focusing manner becomes nearly impossible when measuring a moving sample or dynamic processes. In DHM, the difficulty in mechanical focusing is circumvented by a refocusing process: propagating an object wave from hologram plane to image plane. Notably, the DHM enables to refocus laterally-separated regions of a hologram to different focal planes and consequently, it can provide 3D information of the sample.[6] A key issue in reconstructing a refocused image from the out-of-focus hologram is the image plane determination, i.e., to find the distance between the hologram plane and the image plane. Hitherto, there have been many reports on image plane detection, which are based on amplitude analysis,[7–9] intensity gradient,[10] self-entropy,[11] local intensity variance,[12] spectral norms,[13] wavelet theory,[14] and so on.[15–20] Recently, we also reported non-conventional illumination based image plane determination approaches, which are based on two-wavelength illumination,[21] off-axis illuminations[22] or structured illumination.[23] The image plane was determined by finding the minimal difference between the reconstructed object waves which are aligned with two wavelength illuminations, two off-axis illuminations, or two diffraction orders of structured illumination.

In aside of the image plane determination, the non-conventional illumination schemes[21–26] enable an increased data acquisition along the designed illuminations. Normally, DHM uses a plane wave for illumination and consequently, its resolution and axial sectioning ability of DHM is worse than that of the conventional microscope, which employs Koehler illumination with a boarder spectrum. Off-axis illumination,[22,24] structured illumination[23] and speckle illumination[25,26] can improve the lateral resolution of DHM, and in the meantime contribute to improving the axial sectioning ability of DHM. Recently, opposed-view dark-field digital holographic microscopy was proposed, which collects the scattered light concurrently from both opposite views, and therefore improves the contrast of internal structures and as well the signal-to-noise ratio.[27,28]

In this paper, we present an opposite-view digital holographic microscopy (OV-DHM) for autofocusing and field of view (FOV) extension. The OV-DHM enables to determine the image plane automatically and refocus a sample digitally, providing the possibility to image moving samples or dynamic processes. Compared with conventional autofocusing methods, the presented technique can be used for more general samples. Furthermore,

[1]School of Physics and Optoelectronic Engineering, Xidian University, Xi'an, 710071, China. [2]Institute of Applied Physics, Karlsruhe Institute of Technology, 76128, Karlsruhe, Germany. [3]Institute of Nanotechnology, Karlsruhe Institute of Technology, 76344, Eggenstein-Leopoldshafen, Germany. Correspondence and requests for materials should be addressed to P.G. (email: peng.gao@kit.edu) or X.S. (email: xpshao@xidian.edu.cn)

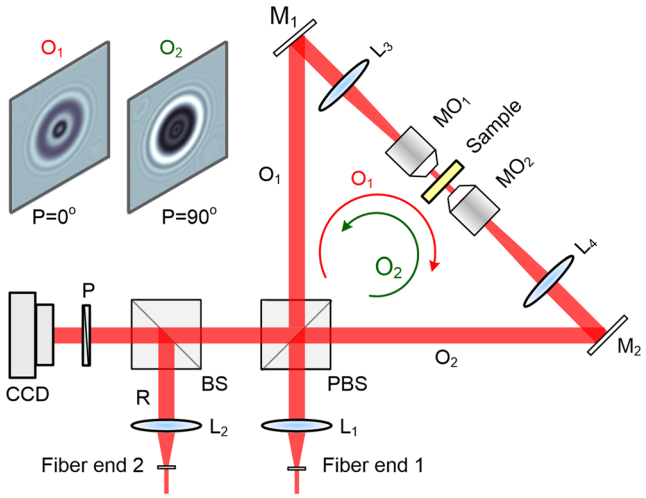

Figure 1. Experimental setup of opposite-view digital holographic microscopy (OV-DHM). MO_1 and MO_2, microscopic objectives; L_1–L_4, achromatic lenses; BS, beamsplitter; PBS, polarization-maintaining beamsplitter; M_1 and M_2, mirrors; P, polarizer; CCD, Charge-coupled device; O_1 and O_2, Object waves linearly polarized along horizontal (0°) and vertical (90°) directions, respectively; R, reference wave linearly polarized at an azimuth of 45°.

OV-DHM can extend the field of view (FOV) of imaging by combining the two reconstructed object waves, which have an angle in-between. Furthermore, OV-DHM can collect more frequency spectrum (from two sides), and thus it has the potential to suppress out-of-focus background.

Results

Configuration of OV-DHM. The schematic diagram of our home-built opposite-view digital holographic microscopy (OV-DHM) is shown in Fig. 1. The experiment setup is based on a common-path Sagnac configuration, which is comprised of a polarization-maintaining beamsplitter PBS and two mirrors M_1 and M_2. A laser beam from the fiber end 1 is split by the PBS into two copies, of which the polarizations are along the horizontal and vertical directions, respectively. The copy which has horizontal polarization goes through the Sagnac configuration clockwise, while the other one goes through the Sagnac configuration anti-clockwise. Two telescope systems MO_1-L_3 and L_4-MO_2 are placed between M_1 and M_2, and are used to image a sample with a magnification of 20X. A sample is located between the objectives MO_1 and MO_2. After the illumination beams transmit the sample in opposite directions, the output object waves (namely O_1 and O_2) are magnified by the two telescope systems, and superimposed with a common reference wave R via a non-polarizing beamsplitter BS. The reference wave is linearly polarized with its polarization azimuth 45° with respect to the polarizations of O_1 and O_2. Two hologram $I_1 = |O_1 + R|^2$ and $I_2 = |O_2 + R|^2$ were obtained separately by rotating the polarizer P to horizontal and vertical directions, respectively. We note that the reference wave R was adjusted to have an angle of 10 ± 0.1 mrad with respect to the two in-line object waves. It is worthy to mention that the OV-DHM configuration can be further upgraded by employing two CCD cameras to record the two opposite-view holograms at the same time (see Supplementary Fig. 1).

Autofocusing principle of the OV-DHM. As seen in Fig. 2(a), a CCD is placed to record the in-focus images of the middle plane P_{mid} of the two objectives clockwise and anti-clockwise in OV-DHM. If a sample is located to have a distance Δz from P_{mid}, the hologram I_1 will have a defocusing distance $M^2\Delta z$ along clockwise direction, while the hologram I_2 will have an opposite defocusing distance $-M^2\Delta z$ along the anti-clockwise direction. Here M is the magnification of the OV-DHM system. For reconstruction, the two object waves, O_{r1} and O_{r2}, which have an arbitrary distance $-\Delta d$ from I_1 (and Δd from I_2) can be reconstructed by using angular spectrum method:[29]

$$\begin{cases} O_{r1} = FT^{-1}\left\{FT\{I_1R_D\} \cdot W_{filter} \cdot \exp[-ik\Delta d\sqrt{1 - (\lambda\xi)^2 - (\lambda\eta)^2}]\right\}, \\ O_{r2} = FT^{-1}\left\{FT\{I_2R_D\} \cdot W_{filter} \cdot \exp[ik\Delta d\sqrt{1 - (\lambda\xi)^2 - (\lambda\eta)^2}]\right\}. \end{cases} \quad (1)$$

Here $k = 2\pi/\lambda$ denotes the wave vector; $FT\{\cdot\}$ and $FT^{-1}\{\cdot\}$ denote Fourier-transformation and inverse Fourier-transformation operators, ξ and η are the spatial coordinates in the frequency domain. R_D is a digitalized reference waves, which has a linear phase term (corresponding to the angle between object wave and reference wave) used to shift the spectrum of the real image to the center of the frequency domain. $W_{filter}(\xi, \eta)$ is the window function used to select the real images of I_1R_D and I_2R_D in the frequency domain, blocking their dc terms and twin images (see Supplementary Fig. S2). The cut-off frequency of W_{filter} was chosen to maintain the highest frequency of the object wave (defined with ω_0). The angle between the object and reference waves should be designed to

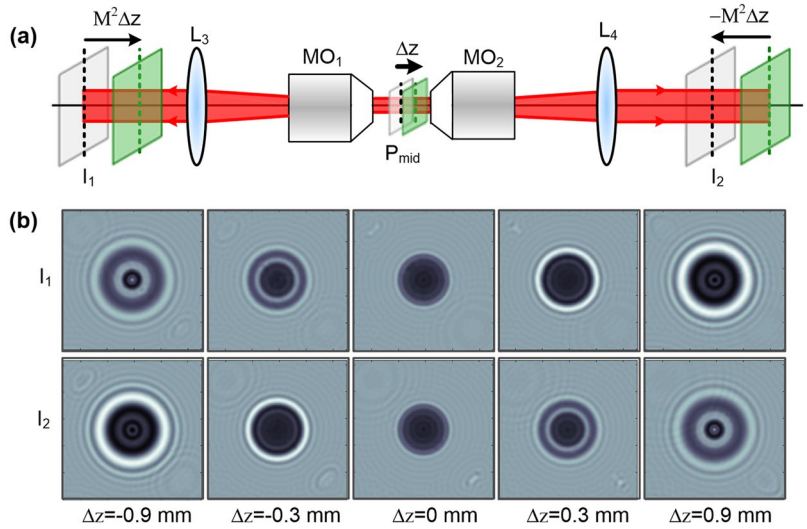

Figure 2. Schematics of autofocusing of OV-DHM. (**a**) Illumination and imaging schematics of OV-DHM; P_{mid} denotes the middle plane of telescope system MO_1-L_3 and MO_2-L_4; M denotes the magnification of the two telescope systems. (**b**) The simulated images of a sample on CCD plane when it moves from left to right with $\Delta z = -0.9$ mm, -0.3 mm, 0 mm, 0.3 mm and 0.9mm from the middle plane P_{mid}.

yield an off-axis hologram which has a carrier frequency $\geq 3\omega_0$ in order to a separation between the real image, twin image and *dc* term.[30] A CCD camera which has a sampling frequency $\geq 8\omega_0$ is required to record the hologram.

OV-DHM has an intrinsic property that, the holograms I_1 and I_2 have opposite defocusing distances. Thus, the difference between $|O_{r1}(\Delta d)|^2$ and $|O_{r2}(-\Delta d)|^2$ reaches the minimum when the reconstruction distance Δd is correct (match $M^2\Delta z$). Otherwise, the larger $|\Delta d - M^2\Delta z|$ is, the larger is the variation of $|O_{r1}(\Delta d)|^2 - |O_{r2}(-\Delta d)|^2$. Thus, this property can be used as focus criterion to determine image plane of OV-DHM. For this purpose, the focus criterion can be defined as:

$$Cri(\Delta d) = RMS\{|O_{r1}|^2 - |O_{r2}|^2\} \quad (2)$$

In Equation (2), *RMS* denotes the operation of root-mean-square operation. In implementation, an in-focus plane can be determined by finding the minimum of the criterion function in Equation (2).

Autofocusing of lensless OV-DHM. Lensless OV-DHM was firstly performed on the configuration sketched in Fig. 1 omitting the imaging units MO_1-L_3 and MO_2-L_4. A structured glass plate which has both amplitude and phase modulations was used as a sample. The sample was located in the plane having 7.5 ± 0.1 cm distance from the plane P_{mid}, which has an equal distance of 40 cm to the CCD plane clockwise and anti-clockwise. Figure 3(a) shows the two holograms I_1 and I_2 obtained by rotating the polarizer P to horizontal and vertical directions. The two object waves (O_{r1} and O_{r2}) were reconstructed and propagated for a distance of -40 cm $\pm \Delta d$ with Δd varying between -20 cm and 20 cm. For each reconstruction distance, the focus criterion defined with Equation (2) was shown in Fig. 3(b). The proposed criterion shows a minimum at $\Delta d = -7.5 \pm 0.2$ cm, which is in good agreement with the prior-set value. Here the error 0.2 cm is the calculation step for digital re-focusing. In contrast, the conventional criterion, e.g., intensity analysis based (IAB) criterion, failed to find the correct image plane. This is because the phase distribution of the object wave introduces additional intensity variation in out-of-focus planes, which balances surpass the intensity variation of the object wave in the image plane. In Fig. 3(c), we show the reconstructed $|O_{r1}|$ and $|O_{r1}| - |O_{r2}|$ at different Δd. It is distinct that the variation between $|O_{r1}|$ and $|O_{r2}|$ becomes minimal at the image plane. In contrast, the intensity modulation of a single object wave, e.g., O_1, does not appear a monistic change with Δd. This, in turn, explains why the conventional IAB criterion can not find the correct image plane. For a sample with both amplitude and phase modulation, the advantage of the proposed method over the conventional autofocusing methods, *i.e.*, integrated amplitude modulus (IAM), Laplace Filtering based differential method (LAP), Variance of intensity distribution (VAR) based methods, has also been verified (see Supplementary Text1 and Supplementary Fig. 3). Eventually, by using the obtained $\Delta d = -7.5 \pm 0.2$ cm, the focused amplitude and phase image of the sample were reconstructed and shown in Fig. 3(d) and (e). A clear area on $|O_{r1}|$, $|O_{r2}|$ and $(|O_{r1}| + |O_{r2}|)/2$, indicated with the green rectangle in Fig. 3(d), were selected for comparison on speckle noise. The standard deviations on their intensity fluctuation 0.30, 0.36 and 0.21 were obtained, implies that speckle noise can be efficiently reduced by averaging the two reconstructed object waves.

Autofocusing of lens-based OV-DHM. Lens-based OV-DHM was firstly carried out on a rectangular-grid target (R155731-09100, Edmund Optics, Barrington, NJ, USA) with sharp absorbing structures, as is shown in Fig. 4(a). After the two opposite-viewed holograms were recorded, the focus criterion of the proposed method

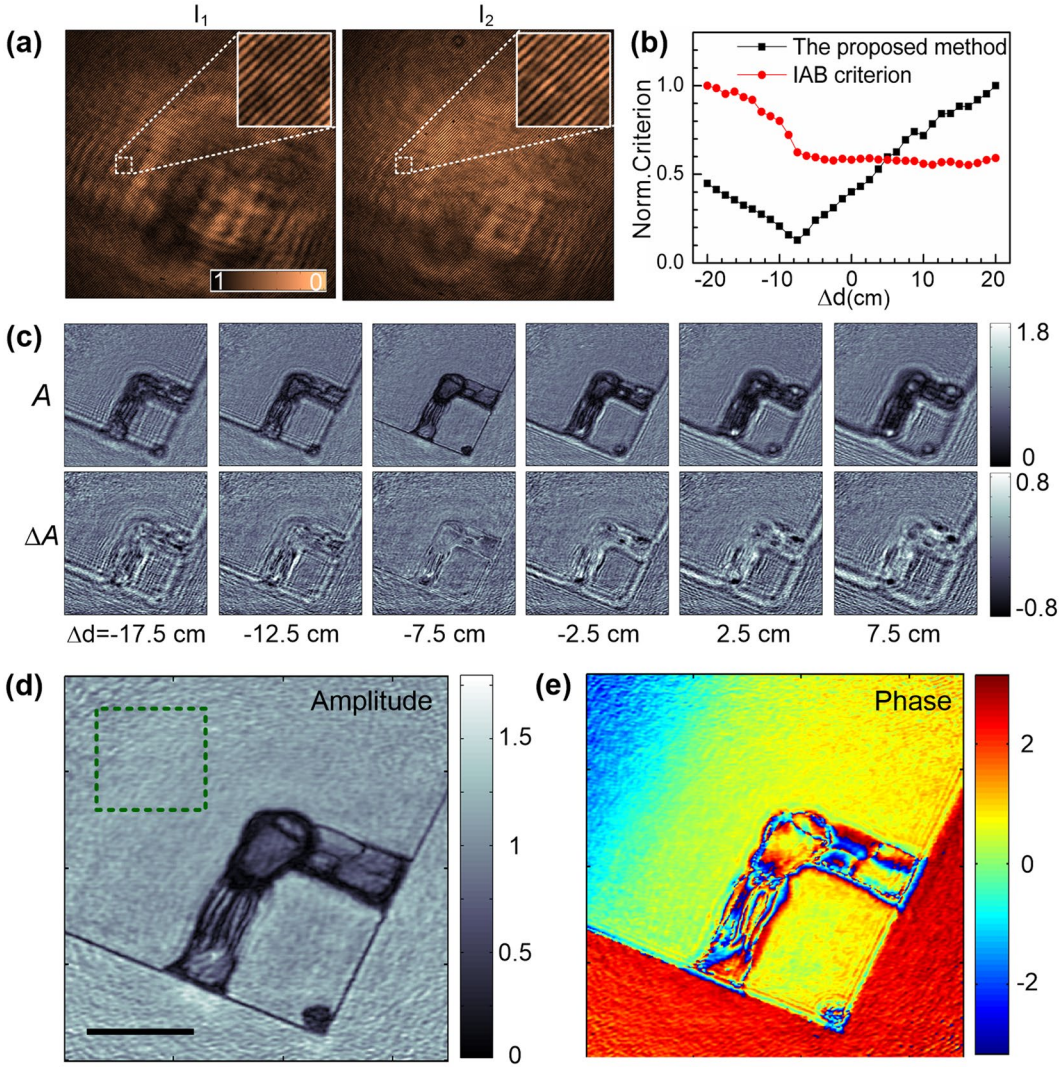

Figure 3. Autofocusing of lensless OV-DHM for a sample with both amplitude and phase modulation. (**a**) Holograms of the sample recorded by rotating the polarizer P to horizontal and vertical directions. The two insets in (**a**) are the zoomed areas indicated with the two dash-white close-ups in (**a**). (**b**) The focus criterion curves of the proposed method and a conventional focus criterion: intensity analysis based method (IAB method). (**c**) Reconstructed amplitude A of O_1 (top) and, the difference ΔA between $|O_1|$ and $|O_2|$ (bottom). (**d**) Averaged amplitude and (**e**) phase distributions of O_1 and O_2 reconstructed with $\Delta d = 40 \pm 7.5$ cm. Scale bar in (**d**), 1 mm. The green close-up in (**d**) indicate the area on which speckle noise level is evaluated for O_1, O_2, and $(O_1 + O_2)/2$, respectively.

was calculated and compared with the focus criterion (IAM)[7] in Fig. 4(b). The IAM method determined the image plane at $\Delta z = 95$ μm with which the amplitude modulus is minimized for an amplitude object. The proposed criterion tells the focus plane at $\Delta z = 89$ μm. The deviation between the two methods 6 μm is within the range of the depth of field (DOF) of the imaging system ($2\lambda/NA^2 = 7\mu m$). To follow up, the lens-based OV-DHM was carried out for microscopic biological sample. Human HeLa cells (LGC Standards GmbH, Wesel, Germany) sat on a coverslip surface and covered with another coverslip was used as a microscopic sample. Figure 5(a) shows the two opposite-view holograms I_1 and I_2, and the zoomed areas of I_1 and I_2 highlight the dense fringes due to the angle between the object wave and the reference wave. After calculated with Equation (2), the focus criterion in Fig. 5(b) shows a minimum at $\Delta z = -180 \pm 5$ μm, which was further verified by Fig. 5(c) where the amplitude difference O_{r1} and O_{r2} reaches its minimum at $\Delta z = -180$ μm. By using the obtained Δz, the amplitude and phase images of the HeLa cells were reconstructed and shown in Fig. 5(d) and (e), respectively. The comparison between Fig. 5(d) and (e) reveals that phase image of these HeLa cells has higher contrast compared with their amplitude/intensity image, which is available with a conventional microscope. We note that the refractive index of the cell can be further determined by using the method proposed in refs 31 and 32.

Field Of View (FOV) extension by OV-DHM. The OV-DHM has also the ability to extend the field of view (FOV) of phase imaging. To achieve this purpose, the two object waves were aligned to have an angle

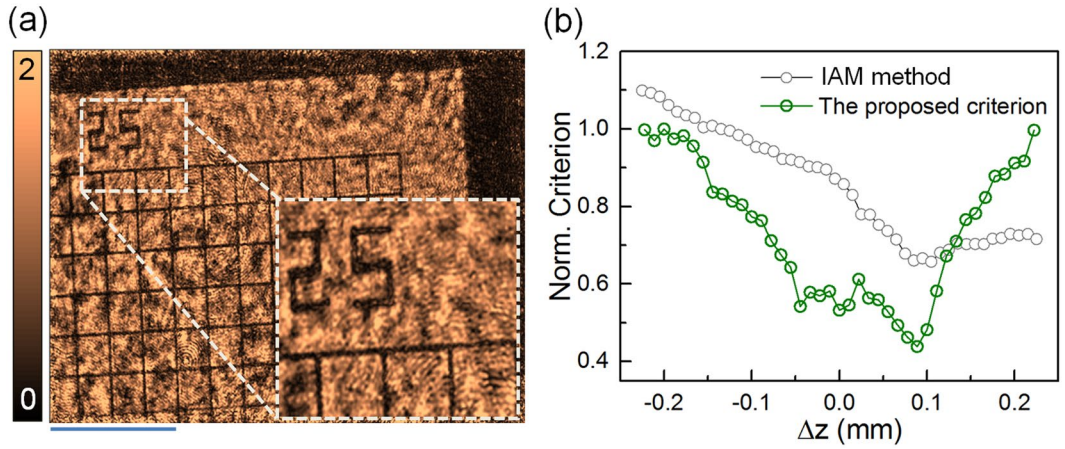

Figure 4. OV-DHM for amplitude sample. (**a**) Reconstructed amplitude of the sample; scale bar 75 μm; the inset in (**a**) shows the zoomed image of the rectangular area indicated with the dash square. (**b**) Focus criterion curves calculated with the proposed method and the integrated amplitude modulus based method, for which the integral of the amplitude modulus is minimized when the focused plane is reached[6].

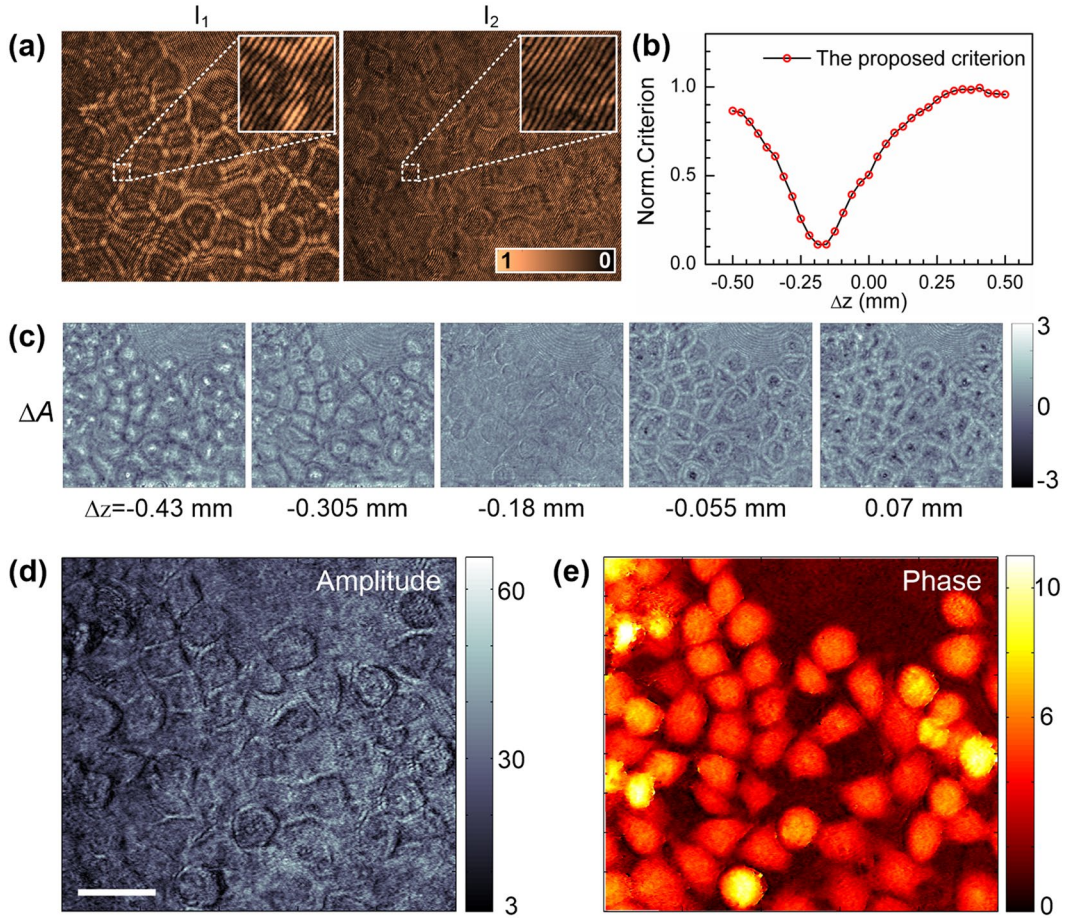

Figure 5. OV-DHM for Hela cells. (**a**) Two opposite-view holograms of the two object waves O_1 and O_2. Insets show the zoomed rectangular areas within the white close-ups in (**a**). (**b**) Focus criterion curves calculated with the proposed method. (**c**) The difference between the amplitudes of $|O_1|$ and $|O_2|$. (**d**) Reconstructed amplitude and (**e**) phase of the object wave O_1. Scale bar in (**d**), 45 μm.

α in-between (after magnified by the objectives). By doing this, the CCD camera recorded different parts of the sample image/diffraction pattern along two object waves (see Fig. 6(a) and (b)). In this case, image plane determination can still be performed by replacing $|O_{r1}(x,y,\Delta d)|^2 - |O_{r2}(x, y, -\Delta d)|^2$ in Equation (2) with $|O_{r1}(x,$

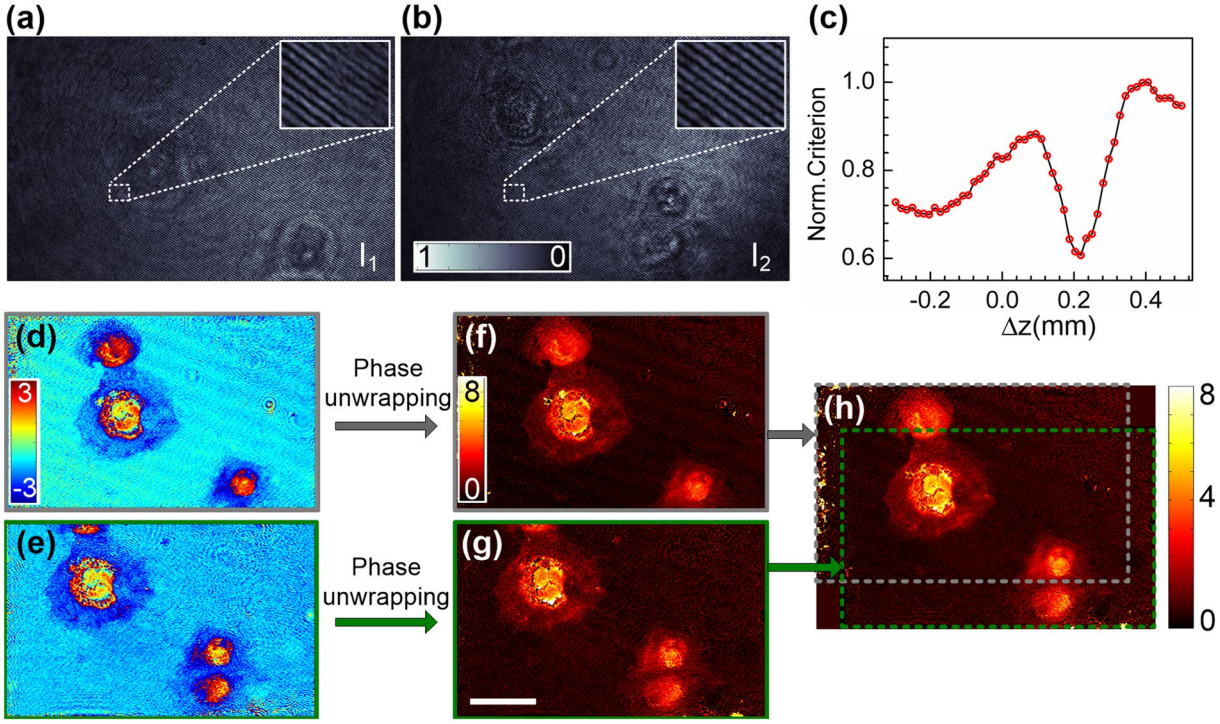

Figure 6. Extension of field of view (FOV) by OV-DHM. (**a**) and (**b**) opposite-view holograms of Cos7 cells (Sigma-Aldrich, St. Louis, MO); (**c**) criterion for image plane determination; (**d**) and (**e**) wrapped phase of O1 and O2; (**f**) and (**g**) unwrapped phases of O1 and O2; by using the Goldstein phase-unwrapping algorithm;[32] (**h**) combined phase image for field of view (FOV) extension. The phase value in (**f**)–(**h**) is reversed for a better display contrast. Scale bar in (**g**), 90 μm.

$y + [\tan(\alpha/2)]\Delta d, \Delta d)|^2 - |O_{r2}(x, y - [\tan(\alpha/2)]\Delta d, -\Delta d)|^2$, supposing the angle between the two object waves is in y direction (the angle can be in any direction). The focus criterion was calculated from the central area where the two opposite-view object waves are overlapped, and the result was shown in Fig. 6(c), from which the reconstruction distance $\Delta d = M^2\Delta z = 8.4 \pm 0.2$ cm was obtained. The phase images of O_1 and O_2 reconstructed with $\Delta d = 8.4$ cm were shown in Fig. 6(d) and (e), and the counterparts after phase unwrapping operation[33] were in Fig. 6(f) and (g). It can be seen that the two phase images exhibit different parts of the tested sample. After the two images were combined together, the whole field of view is extended from 1.2×10^5 μm^2 to 1.6×10^5 μm^2 in Fig. 6(h); that said, 30% FOV extension was achieved by the OV-DHM. The combined image shows Cos7 cells proliferation status: one to two after 24 hours relocation on a glass plate. The phase image also confirms that the nucleus is much denser in refractive index than that of cytosol in a cell.

Discussions

In this paper, opposite-view digital holographic microscopy (OV-DHM) was presented for autofocusing and field of view (FOV) extension. The out-of-focusing distance (a distance between the image plane and CCD plane) is determined by searching the minimal difference between two object waves reconstructed from two opposite-view holograms. Based on this distance, refocusing of the sample has been performed by propagating the reconstructed object waves to their common image plane. Compared with the conventional image plane determination methods, this method does not rely on the type of a sample (i.e., can be used for the sample with both amplitude and phase modulations). This advantage is due to the intrinsic illumination scheme of OV-DHM and is valid for both lensless OV-DHM and lens-based OV-DHM. The autofocusing can be performed on different regions of the sample: by refocusing and resorting different laterally-separated regions of a sample into their correct axial planes, a 3D image of the sample can be obtained (Supplementary text 4 and Supplementary Figs 4–6). Furthermore, averaging the two object waves can also contribute to suppressing the out-of-focusing background, since only the in-focus components (e.g., cells) appear the same in the two images, wherever the out-of-focus components have different defocusing distance in the two images (see Supplementary Figs 5 and 6).

In case there is an angle between the two opposite-view object waves, extension of the field of view (FOV) can be performed by combining the two reconstructed images. Since the lateral shift of the two reconstructed object waves has a linear relation with the defocusing distance,[22] out-of-focus information and speckle noise can be suppressed by averaging the two object waves (Supplementary Figs 5 and 6). Furthermore, the angle between the two illuminations has also the potential to improve the lateral resolution of the OV-DHM, considering a larger spectrum can be synthesized by combining the spectra of the two off-axis propagated object waves[22–24]. It is worthy to notice that there is a conflict between FOV extension and the improvement on sectioning and resolution improvement, since they rely on different experimental setting. To extend the FOV, the sample should be placed

has a certain distance Δz from the middle plane of the two objectives (which corresponds to the in-focus plane). This defocus distance Δz will provide a lateral shift of $2\tan(\alpha/2)M^2\Delta z$ between two opposite-view images in CCD/CMOS plane, which is used for FOV extension. Whereas, to improve the resolution and sectioning ability, a sample (or a section of it) should be located in the middle plane of the two objectives, where the two object waves will have the same image on CCD/CMOS plane. The potential of OV-DHM on improving section ability could be further explored by using two coherent opposite-view illuminations to generate a structured illumination with in the axial direction, similar to I^5M microscope.[34] Furthermore, the two object waves with orthogonal polarizations have also the potential to provide polarization-resolved information for the anisotropic sample[35].

The OV-DHM has also the following disadvantages: firstly, the configuration of the OV-DHM is far more complex than that of the convention DHM, and the requirement of two opposite-view object waves makes it not compatible with a common microscope frame. Secondly, the autofocusing of OV-DHM requires symmetry on two opposite-view object waves. Thus, the two waves should be aligned carefully, and collimated well to avoid defocusing and other aberrations.

Methods

OV-DHM Setup and alignment. The OV-DHM setup was constructed according to the sketch in Fig. 1. For the lensless OV-DHM mode, the imaging units MO_1-L_3 and MO_2-L_4 was omitted. The middle plane of the mirror M_1 and M_2 has the same distance 40 cm to the CCD plane along clockwise and anti-clockwise directions. For the lens-based OV-DHM mode, two telescope systems MO_1-L_3, and MO_2-L_4, were used to image samples with a magnification of 20x. MO_1 and MO_2 are two identical, plan-field microscopic objectives (Plan 25X/0.4, Nanjing Yingxing Optical Instrument Company, Nan Jing, China). L_3 and L_4 are the achromatic lens (AC254-200-A-ML, Thorlabs GmbH, Munich, Germany) with focal length 200 mm and diameter 1 inch. An additional telescope system with a magnification M = 1.5 was placed before the CMOS camera to further magnify the object waves.

The following procedure can be performed to make the two opposite-view object waves along the same line: A circular aperture (diameter: 2 mm) was located in the center of the input beam before the polarization beam-splitter PBS (PBS251, Thorlabs GmbH, Munich, Germany). Then, adjust the mirror M_2 to make sure the two circular patterns (of the clockwise-propagated and anti-clockwise-propagated beams) on the mirror M_1 are overlapped. Similarly, adjust the mirror M_1 to make sure the two circular patterns on the mirror M_2 are overlapped. In addition, the angle between the in-line object waves (O_1 and O_2) and the reference wave was set to 10 ± 0.3 mrad, which was evaluated by Fourier analysis on the off-axis hologram[36]. The generated off-axis hologram was recorded by a Complementary metal–oxide–semiconductor (CMOS) camera (1920 × 1200pixels, 5.86 μm/pixel, 54 fps, DMK 23UX174, Imaging Source, Bremen, Germany). In the reconstruction of the hologram, an asymmetric window function $W_{filter}(\xi,\eta)$ was used to collect more high-frequency spectrum in the directions other than the carrier-frequency direction (see Supplementary Fig. 2).

Compared to an in-focus recording hologram, the out-of-focus recording hologram requires increased spatial bandwidth product (SBP), and the SBP consumption increases with the out-of-focus recording distance.[37,38] We note that this requirement can be released by using a larger magnification in the OV-DHM system or utilizing a Slightly-off-axis[4,30] and on-axis[39,40] recording scheme. In our experiment, a CCD with pixel size 1/4.4 AU (airy unit, the diameter of the first-order diffraction-limited Airy disc in CCD plane) was used, with which a slight resolution reduction still happen in the case of a large out-of-focus distance. Thus, in order to avoid the SBP deficit and high-frequency cutting by the objective, we limited the out-of-focusing distances in a range of $[-wd/10, wd/10]$, with the wd being the working distance of the used objective.

Numerical compensation for axial misalignment of OV-DHM. In the lens-based OV-DHM, The two telescope systems were aligned such that the clockwise and anti-clockwise images of the middle plane P_{mid} (of the two objectives MO_1 and MO_2) have a defocusing distance of 6 cm and 0 cm on the CCD. For numerical compensation, the reconstruction distance $\Delta d - 0.06$ m and $-\Delta d$ were used (instead of Δd and $-\Delta$d) in Equation (2) for image plane determination of O_{r1} and O_{r2}.

Cell culture and sample preparation. The preparation of the biological samples has followed the protocol in the literature[41]. Human HeLa cells (LGC Standards GmbH, Wesel, Germany) and COS-7 cells (Sigma-Aldrich, St. Louis, MO) were maintained at 37 °C and 5% CO_2 in Dulbecco's modified Eagle's medium (DMEM), containing 10% fetal bovine serum (FBS) and antibiotics (60 μg/mL penicillin and 100 ng/mL streptomycin, both from Invitrogen, Carlsbad, Canada). 24 h after seeding the cells on cover glasses which was placed in the bottom of a plastic-disc container and cultured with the aforesaid medium.

References

1. Cuche, E., Marquet, P. & Depeursinge, C. Spatial filtering for zero-order and twin-image elimination in digital off-axis holography. *Appl. Opt.* **39**, 4070–4075 (2000).
2. Kemper, B. & Bally, G. V. Digital holographic microscopy for live cell applications and technical inspection. *Appl. Opt.* **47**, A52–A61 (2008).
3. Osten, W. *et al.* Recent advances in digital holography. *Appl. Opt.* **53**, G44–G63 (2014).
4. Gao, P. *et al.* Parallel two-step phase-shifting digital holographic microscopy based on a grating pair. *J. Opt. Soc. Am. A* **28**, 434–440 (2011).
5. Langehanenberg, P., Kemper, B., Dirksen, D. & von Bally, G. Autofocusing in digital holographic phase contrast microscopy on pure phase objects for live cell imaging. *Appl. Opt.* **47**, D176–D182 (2008).
6. Kemper, B. *et al.* Integral refractive index determination of living suspension cells by multifocus digital holographic phase contrast microscopy. *J. Biomed. Opt.* **12**, 054009 (2007).

7. Dubois, F., Schockaert, C., Callens, N. & Yourassowsky, C. Focus plane detection criteria in digital holography microscopy by amplitude analysis. *Opt. Express* **14**, 5895–5908 (2006).
8. Antkowiak, M., Callens, N., Yourassowsky, C. & Dubois, F. Extended focused imaging of a microparticle field with digital holographic microscopy. *Opt. Lett.* **33**, 1626–1628 (2008).
9. Memmolo, P. *et al.* Automatic focusing in digital holography and its application to stretched holograms. *Opt. Lett.* **36**, 1945–1947 (2011).
10. Yu, L. & Cai, L. Iterative algorithm with a constraint condition for numerical reconstruction of a three dimensional object from its hologram. *J. Opt. Soc. Am. A* **18**, 1033–1045 (2001).
11. Gillespie, J. & King, R. A. The use of self-entropy as a focus measure in digital holography. *Pattern Recognit. Lett* **9**, 19–25 (1989).
12. Ma, L. H., Wang, H., Li, Y. & Jin, H. Z. Numerical reconstruction of digital holograms for three-dimensional shape measurement. *J. Opt. A: Pure Appl. Opt.* **6**, 396–400 (2004).
13. Li, W., Loomis, N. C., Hu, Q. & Davis, C. S. Focus detection from digital in-line holograms based on spectral l1 norms. *J. Opt. Soc. Am. A* **24**, 3054–3062 (2007).
14. Liebling, M. & Unser, M. Autofocus for digital Fresnel Holograms by use of a Fresnelet-Sparsity Criterion. *J. Opt. Soc. Am. A* **21**, 2424–2430 (2004).
15. Lee, S., Lee, J. Y., Yang, W. & Kim, D. Y. Autofocusing and edge detection schemes in cell volume measurements with quantitative phase microscopy. *Opt. Express* **17**, 6476–6486 (2009).
16. Tachiki, M. L., Itoh, M. & Yatagai, T. Simultaneous depth determination of multiple objects by focus analysis in digital holography. *Appl. Opt.* **47**, D144–D153 (2008).
17. Lebrun, D., Benkouider, A., Coetmellec, S. & Malek, M. Particle field digital holographic reconstruction in arbitrary tilted planes. *Opt. Express* **11**, 224–229 (2003).
18. Park, Y., Popescu, G., Badizadegan, K., Dasari, R. R. & Feld, M. S. Fresnel particle tracing in three dimensions using diffraction phase microscopy. *Opt. Lett.* **32**, 811–813 (2007).
19. Sheng, J., Malkiel, E. & Katz, J. Digital holographic microscope for measuring three-dimensional particle distributions and motions. *Appl. Opt.* **45**, 3893–3901 (2006).
20. Javidi, B., Yeom, S., Moon, I. & Daneshpanah, M. Real-time automated 3D sensing, detection, and recognition of dynamic biological micro-organic events. *Opt. Express* **14**, 3806–3829 (2006).
21. Gao, P. *et al.* Autofocusing based on wavelength dependence of diffraction in two-wavelength digital holographic microscopy. *Opt. Lett.* **37**, 1172–1174 (2012).
22. Gao, P. *et al.* Autofocusing of digital holographic microscopy based on off-axis illuminations. *Opt. Lett.* **37**, 3630–3632 (2012).
23. Gao, P., Pedrini, G. & Osten, W. Structured illumination for resolution enhancement and autofocusing in digital holographic microscopy. *Opt. Lett.* **38**, 1328–1330 (2013).
24. Yuan, C. J., Situ, G., Pedrini, G., Ma, J. & Osten, W. Resolution improvement in digital holography by angular and polarization multiplexing. *Appl. Opt.* **50**, B6–11 (2011).
25. Almoro, P. F. & Hanson, S. G. Object wave reconstruction by speckle illumination and phase retrieval. *J. Eur. Opt. Soc.* **4**, 09002-1-7 (2009).
26. Almoro, P., Pedrini, G. & Osten, W. Aperture synthesis in phase retrieval using a volume-speckle field. *Opt. Lett.* **32**, 733–735 (2007).
27. Faridian, A., Pedrini, G. & Osten, W. Opposed-view dark-field digital holographic microscopy. *Biomed. Opt. Express* **5**, 728–736 (2014).
28. Faridian, A., Pedrini, G. & Osten, W. High-contrast multilayer imaging of biological organisms through dark-field digital refocusing. *J. Biomed. Opt.* **18**, 086009 (2013).
29. Zheng, J. *et al.* Fluorescence volume imaging with an axicon: simulation study based on scalar diffraction method. *Appl. Opt.* **51**, 7236–7245 (2012).
30. Shaked, N. T., Zhu, Y., Rinehart, M. T. & Wax, A. Two-step-only phase-shifting interferometry with optimized detector bandwidth for microscopy of live cells. *Opt. Express* **17**, 15585–15591 (2009).
31. Kemper, B. *et al.* Investigation of living pancreas tumor cells by digital holographic microscopy. *J. Biomed. Opt.* **11**, 34005 (2006).
32. Curl, C. L. *et al.* Refractive index measurement in viable cells using quantitative phase-amplitude microscopy and confocal microscopy. *Cytometry A* **65**, 88–92 (2005).
33. Goldstein, R. M., Zebken, H. A. & Werner, C. L. Satellite radar interferometry: Two-dimensional phase unwrapping. *Radio Sci.* **23**, 713–720 (1988).
34. Gustafsson, M. G. L., Agard, D. A. & Sedat, J. W. I5M: 3D widefield light microscopy with better than 100 nm axial resolution. *J. Microsc.* **195**, 10–16 (1999).
35. Hristu, R., Stanciu, S. G., Tranca, D. E. & Stanciu, G. A. Improved quantification of collagen anisotropy with polarization-resolved second harmonic generation microscopy. *J. Biophoton* **10**, 00197, doi:10.1002/jbio201600197 (2016).
36. Min, J. W. *et al.* Simple and fast spectral domain algorithm for quantitative phase imaging of living cells with digital holographic microscopy. *Opt. Letts.* **42**, 227–230 (2017).
37. Stern, A. & Javidi, B. Space-bandwidth conditions for efficient phase-shifting digital holographic microscopy. *J. Opt. Soc. Am. A* **25**, 736–741 (2008).
38. Claus, D. & Iliescu, D. Optical parameters and space-bandwidth product optimization in digital holographic microscopy. *Appl. Opt.* **52**, A410–A422 (2013).
39. Yamaguchi, I. & Zhang, T. Phase-shifting digital holography. *Opt. Lett.* **22**, 1268–1270 (1997).
40. Gao, P. *et al.* Phase-shift extraction for generalized phase-shifting interferometry. *Opt. Lett.* **34**, 3553–3555 (2009).
41. Gao, P., Prunsche, B., Zhou, L., Nienhaus, K. & Nienhaus, G. U. Background suppression in fluorescence nanoscopy with stimulated emission double depletion. *Nat. Photon* **11**, 163–169 (2017).

Acknowledgements

The authors would like to thank Prof. Wolfgang Osten and Dr. Giancarlo Pedrini from University Stuttgart for the conception of this work. This research was supported by National Natural Science Foundation of China (NSFC) under Grants number. 61605150, 61475187, 61575154, 61107003, U1304617; and the Fundamental Research Funds for the Central Universities under Grants No. JB160511, XJS16005 and JBG160502.

Author Contributions

J.J.Z. and P.G. constructed the OV-DHM setup, performed measurements and analyzed data. P.G. and X.P.S. wrote the manuscript.

Additional Information

Supplementary information accompanies this paper at doi:10.1038/s41598-017-04568-x

Competing Interests: The authors declare that they have no competing interests.